Hindawi
Mathematical Problems in Engineering
Volume 2022, Article ID 8227124, 16 pages
https://doi.org/10.1155/2022/8227124

Research Article

Bifurcation Analysis of Travelling Waves and Multi-rogue Wave Solutions for a Nonlinear Pseudo-Parabolic Model of Visco-Elastic Kelvin-Voigt Fluid

Sabur Uddin,[1,2] **Shazia Karim**,[3] **F. S. Alshammari**,[4] **Harun-Or Roshid**,[1] **N. F. M. Noor**,[5] **Fazlul Hoque**,[1] **Muhammad Nadeem**,[6] **and Ali Akgül**[7,8]

[1]*Department of Mathematics, Pabna University of Science and Technology, Pabna 6600, Bangladesh*
[2]*Department of Applied Mathematics, Gono Bishwabidyalay, Savar, Dhaka, Bangladesh*
[3]*Department of Basic Sciences FSD Campus, UET, Lahore, Pakistan*
[4]*Department of Mathematics, College of Science and Humanities in Al-Kharj, Prince Sattam Bin Abdulaziz University, Al-Kharj 11942, Saudi Arabia*
[5]*Institute of Mathematical Sciences, Faculty of Science, Universiti Malaya, Kuala Lumpur 50603, Malaysia*
[6]*School of Mathematics and Statistics, Qujing Normal University, Qujing 650011, China*
[7]*Siirt University, Art and Science Faculty, Department of Mathematics, Siirt 56100, Turkey*
[8]*Near East University, Mathematics Research Center, Department of Mathematics, Near East Boulevard, PC 99138, Nicosia/Mersin 10, Turkey*

Correspondence should be addressed to F. S. Alshammari; f.alshammari@psau.edu.sa and Harun-Or Roshid; harunorroshidmd@gmail.com

Received 14 May 2022; Accepted 31 August 2022; Published 27 September 2022

Academic Editor: Adnan Maqsood

Through this article, we focus on the extension of travelling wave solutions for a prevalent nonlinear pseudo-parabolic physical Oskolkov model for Kevin-Voigt fluids by using two integral techniques. First of all, we explore the bifurcation and phase portraits of the model for different parametric conditions via a dynamical system approach. We derive smooth waves of the bright bell and dark bell, periodic waves, and singular waves of dark and bright cusps, in correspondence to homoclinic, periodic, and open orbits with cusp, respectively. Each orbit of the phase portraits is envisaged through various energy states. Secondly, with the help of a prevalent unified scheme, an inventive version of exact analytic solutions comprising hyperbolic, trigonometric, and rational functions can be invented with some collective parameters. The unified scheme is an excitably auspicious method to procure novel interacting travelling wave solutions and to obtain multipeaked bright and dark solitons, shock waves, bright bell waves with single and double shocks, combo waves of the bright-dark bell and dark-bright bell with a shock, dark bell into a double shock wave, and bright-dark multirogue type wave solutions of the model. The dynamics of the procured nonlinear wave solutions are also presented through 2-D, 3-D, and density plots with specified parameters.

1. Introduction

Recently, discoveries of novel explicit and analytical travelling wave solutions of nonlinear models have attracted great attention from blooming scientists [1–3]. A series of travelling wave exact solutions with various nonlinear dynamics can be illustrated as unique complex phenomena in diverse scopes of nonlinear sciences, for instance, optics [1–3], fluid mechanics [4, 5], shallow water wave and magneto-sound transmission in plasmas [6], ion-acoustic plasma waves [7, 8], shallow water waves [9, 10], solid-state physics and chemical kinetics [11], visco-elastic Kelvin Voigt fluid [12], shallow water propagation in the harbor and coastal region [13], and nonlinear quantum field theory [14] . Due to the significance of such field of studies, theoretical probes on physical action emulation of NEEs are sought day by day. Hence, much effort has been devoted to

securing exact and analytical travelling wave solutions of the NEEs. Many scholars are compelled by NEEs to raise travelling wave solutions by implementing a number of integral approaches. These approaches that are accomplished in current literature include the extended Kudryashov method [1], the first-integral method [2], the extended trial equation method [3], Bäcklund transformation [4, 5], the extended simple equation method [6], modified simple equation method [7, 8], Hirota bilinear form [9, 10], new generalized (G'/G) -expansion method [11], (G'/G) -expansion method [14], the extended (G'/G)-expansion method [15], Cole-Hopf transformation method [16], Adomian decomposition method [17], $\exp(-\varphi(\xi))$-expansion method [18–20], planner dynamical system scheme [21, 22] and many more.

Among the above procedures, the planner dynamical scheme is the most important, stable, and reliable approach as it provides various types of phase orbits. Depending on the parametric conditions, each type of orbit (periodic, heteroclinic, and homoclinic) yields periodic, kink, and bell wave solutions, respectively, under selective initial/boundary conditions. This type of approach is still least explored on numerous nonlinear models; hence, it breeds a vast challenge for proximate ascertainment of the models' dynamical behaviors. The $(1+1)$-dimensional Oskolkov model for Kevin-Voigt fluids is one of the nonlinear models [23–25] with huge applications in contemplating incompressible visco-elastic Kelvin-Voigt fluid flows. This category of the pseudo-parabolic model, which involves time derivative in the highest differential term, can also be exemplified for wider purviews such as fluid flows of fissured rock, second order shear of fluids, thermodynamics, consolidation of dust, and transmission of long wave propagations with small amplitudes. Hence, the Oskolkov model is anticipatorily examined via diverse schemes by various researchers across the globe [23–25]. Several fundamental and featured procedures have also been established to procure the exact solutions of the Oskolkov model.

The modified simple equation method [12] was used to derive more exact and explicit solutions of the Oskolkov model. The tanh-coth method [23] was applied to accomplish exact solutions of the nonlinear pseudo-parabolic model. Asymptotic stable and unstable solutions to the Oskolkov model were analyzed graphically too [24]. The nonlinear shock wave, bell wave, and various dynamical motions in the presence of an exotic periodic force were discussed briefly for the generalized Oskolkov model [25]. Although the enormous investigation and profound dynamical solutions to the model have been scrutinized by many researchers, there are still some unresolved problems like bounded travelling wave solutions with their corresponding phase orbit, solutions with boundary conditions, and rogue wave solutions. All these updates spark inquisitions on how the results are exhibited and how they vary with the changing parameters. To retort such accounts, we need to derive solutions involving some of the prominent parameters with suitable initial/boundary conditions.

Through this article, we shed light on the progress of nonlinear travelling waves such as bright and dark bell waves, periodic waves, and singular bright and dark cusp waves as corresponding to each orbit of the phase portraits on the dynamical Oskolkov model by utilizing the planner dynamical strategy [20, 21]. Besides, rogue waves, multisoliton, interaction of solitons, and breather wave solutions, which are no less fascinating, have also received gradually increased attention in the field of nonlinear dynamical systems [26–28]. The long wave limit of the breather localized wave was derived by Yue et al. [29]. Abundant research on these topics has been performed and different types of nonlinear localized waves have been revisited for strategic recipes of various nonlinear physical models materialized in mathematical physics and engineering applications [30, 31]. The Haar wavelet technique has been used to analyze the dynamical phenomena of the fractional-order nonlinear model [32, 33]. Nowadays, investigations on the fractional model are studied by analytical techniques [34, 35] and numerically [36, 37], exposing huge efforts. Notwithstanding, we also aim to construct the solutions to multirogue type waves, shock waves, interactions of bright-dark and dark-bright bell solitons, interactions of shock-bell waves, and singular multisoliton to the $(1+1)$-dimensional Oskolkov model by taking benefit of the lavish unified method [38, 39].

The creation of this article is designed as follows: in Section 2, we deliberate the bifurcation and phase portrait analyses of the Oskolkov model. In Section 3, we exhibit parametric expressions of explicit solutions of the Oskolkov model. The exact wave solutions and their graphical illustrations of the model via the unified method are presented in Section 4. Finally, the perspectives of the current study on this kind of dynamical wave phenomenon are discussed in the last section.

2. Bifurcations and Phase Portraits of the Oskolkov Model

The regular form of the $(1+1)$ dimensional Oskolkov model (1) is

$$U_t - \beta U_{xxt} - \alpha U_{xx} + UU_x = 0, \tag{1}$$

where $U(x,t) = U(\xi)$ and $\xi = kx - \omega t$ in which k is a constant whereas ω is the wave speed. Now, we reinstate (1) into the form of (ODE) as follows:

$$2k^2\omega\beta U'' - 2\alpha k^2 U' - 2\omega U + kU^2 = 0, \tag{2}$$

where the primes stand for the derivative with respect to ξ

Equation (2) in a concise form can be reformulated as

$$U'' = PU' + QU - RU^2, \tag{3}$$

where $P = \alpha/\omega\beta, Q = 1/\kappa^2\beta, R = 1/2\kappa\omega\beta$, and $R \neq 0$.

This (3) can further be written into a prototype system of differential form

$$\begin{aligned} U' &= V = F(U,V) \\ V' &= PV + QU - RU^2 = G(U,V), \end{aligned} \tag{4}$$

which yields a Hamiltonian

$$H(U,V) = \frac{V^2}{2} - \frac{QU^2}{2} + \frac{RU^3}{3} = \hbar. \tag{5}$$

Next, we attempt to detect the bifurcation of the phase orbits of the dynamical system in (4) with various conditions on the parameters $\alpha, \beta, \kappa, \omega$. From the observation, it is clear that a smooth homoclinic orbit of the system in (4) arises from the smooth solitary waves in equation (1). When the solution of $U(\kappa x - \omega t) = U(\xi)$, $(-\infty < \xi < \infty)$ of the system guarantees $\lim_{\xi \longrightarrow -\infty} U(\xi) = a$ and $\lim_{\xi \longrightarrow \infty} U(\xi) = b$, $U(\xi)$ is said to be homoclinic and heteroclinic orbits for $a = b$ and $a \neq b$ respectively. Normally, a homoclinic orbit of the (4) correlates with a solitary wave solution of the (1) and a heteroclinic orbit of the (4) correlates with a king (antiking) wave solution of the (1). Alike, a periodic orbit of the system in (4) keeps up a correspondence with a periodic travelling wave solution of (1). Therefore, we can explore to locate all possible phase portraits of the dynamical system in (4) with the help of different constraints on the parameters $\alpha, \beta, \kappa, \omega$.

For critical points in an equilibrium situation, we have to consider $U' = 0$ and $V' = 0$ then that prototype (4) will provide two equilibrium points $\mathrm{N}_0(0, 0)$ and $\mathrm{N}_1(Q/R, 0)$, if $Q \neq 0$. Furthermore, the dynamical prototype (4) yields one equilibrium point $\mathrm{N}(0, 0)$ at $Q = 0$. Now, let us assume, $A(U_\mathrm{N}, V_\mathrm{N})$ to be the coefficients' matrix of the linearized prototype (4) at equilibrium points $\mathrm{N}_i\,(i = 0, 1)$ and let $I = \det A(U_\mathrm{N}, V_\mathrm{N})$. Therefore, we have

$$\begin{aligned} I(\mathrm{N}_0) &= -Q, \\ I(\mathrm{N}_1) &= Q, \\ \mathrm{Trace}(A(\mathrm{N}_0)) &= P, \\ \mathrm{Trace}(A(\mathrm{N}_1)) &= P. \end{aligned} \tag{6}$$

With the help of the bifurcation theorem [21, 22] and the above inspection, we will get the following remarks:

Group-1: for $Q > 0$ the nature at the origin $\mathrm{N}_0(0, 0)$ is a saddle point and $\mathrm{N}_1(Q/R, 0)$ is a center point, whereas the corresponding bifurcations of phase portraits of the prototype (4) are visualized in Figures 1(a) and 1(b), respectively.

Group-2: for $Q < 0$ the nature at origin $\mathrm{N}_0(0, 0)$ is a center point and $\mathrm{N}_1(Q/R, 0)$ is a saddle point, whereas the corresponding bifurcations of phase portraits of the prototype (4) are depicted in Figures 2(a) and 2(b), respectively.

Group-3: for $Q = 0$ the nature at origin $\mathrm{N}_0(0, 0)$ is a cusp point, whereas the corresponding bifurcations of phase portraits of the prototype (4) are depicted in Figures 3(a) and 3(b), respectively.

3. Explicit Expressions of Solution for the Model (1)

In this segment, we derive various explicit parametric illustrations of travelling wave solutions for the model (1). For effortlessness, the energy level of the Hamiltonian is specified as $\hbar_0 = H(0, 0) = 0$ and $\hbar_1 = H(Q/R, 0) = -Q^3/6R^2$.

3.1. Examining Group-1 Based on Figure 1 Observation (Part 2)

(I) For the state $Q > 0$, $R > 0$, the allied homoclinic orbit at $\mathrm{N}_0(0, 0)$ is described via $H(U, V) = \hbar_0$, where the model (1) suggests itself as a valley type smooth solitary wave solution specified by Figure 1(a). Using the relation $H(U, V) = \hbar_0 = 0$ in equation (5), yields

$$V = \pm \sqrt{\frac{2R}{3}}\, U \sqrt{\frac{3Q}{2R} - U}. \tag{7}$$

Combining the first equation of the prototype (4) and (7), we attain the parametric expression of the valley-type smooth solitary wave solution as follows:

$$U(x, t) = \left|\frac{3Q}{2R}\right| \left(1 - \tanh^2\left(\frac{\sqrt{Q}}{2}|\xi|\right)\right), \tag{8}$$

where $\xi = \kappa x - \omega t$, $P = \alpha/\omega\beta, Q = 1/\kappa^2\beta, R = 1/2\kappa\omega\beta$ The profile of the valley solitary wave solution (8) is shown in Figure 4(a) with $a = -1$, $b = 1$, $\omega = 1, \kappa = 1$, $P = -1$, $Q = 1$, $R = 0.5$

(II) For the state $Q > 0$, $R < 0$, it is equivalent to the homoclinic orbit to the stable point at $\mathrm{N}_0(0, 0)$ identified by $H(U, V) = \hbar_0$, where the model (1) suggests itself as a valley-type smooth solitary wave solution portrayed in Figure 1(b). Using the relation $H(U, V) = \hbar_0 = 0$ in equation (5), yields

$$V = \pm \sqrt{-\frac{2R}{3}}\, U \sqrt{-\frac{3Q}{2R} - U}. \tag{9}$$

Combining the first equation of the prototype (5) and (9), we attain the parametric expression of the valley-type smooth solitary wave solution as follows:

$$U(x, t) = \left|\frac{3Q}{2R}\right| \left(\tanh^2\left(\frac{\sqrt{Q}}{2}|\xi|\right) - 1\right), \tag{10}$$

where $\xi = \kappa x - \omega t$, $P = \alpha/\omega\beta, Q = 1/\kappa^2\beta$, $R = 1/2\kappa\omega\beta$ The profile of the valley solitary wave solution (10) is shown in Figure 4(b) with $a = -1$, $b = 1$, $\omega = 1, \kappa = -1, P = -1$, $Q = 1$, $R = -0.5$

(III) For the state $Q > 0$, $R > 0$ or $Q > 0$, $R < 0$, the model (1) represents a set of smooth periodic wave solutions described by $H(U, V) = \hbar$, $\hbar \in (\hbar_1, 0)$ as can be viewed in Figures 1(a) and 1(b), respectively. For the state $Q > 0$, $R > 0$, the phase portrait of the prototype (4) is shown in Figure 1(a). In this phase, the formulation of the closed domain can be written as: $V = \pm \sqrt{2R/3}\, \sqrt{(U - \Theta_1)(\Theta_2 - U)(\Theta_3 - U)}$, (11) where $(\Theta_1, 0)$, $(\Theta_2, 0)$ and $(\Theta_3, 0)$ are the meeting points of the curve identified by the orbits $H(U, V) = \hbar$, $h \in (\hbar_1, 0)$ on the U-axis that pre-

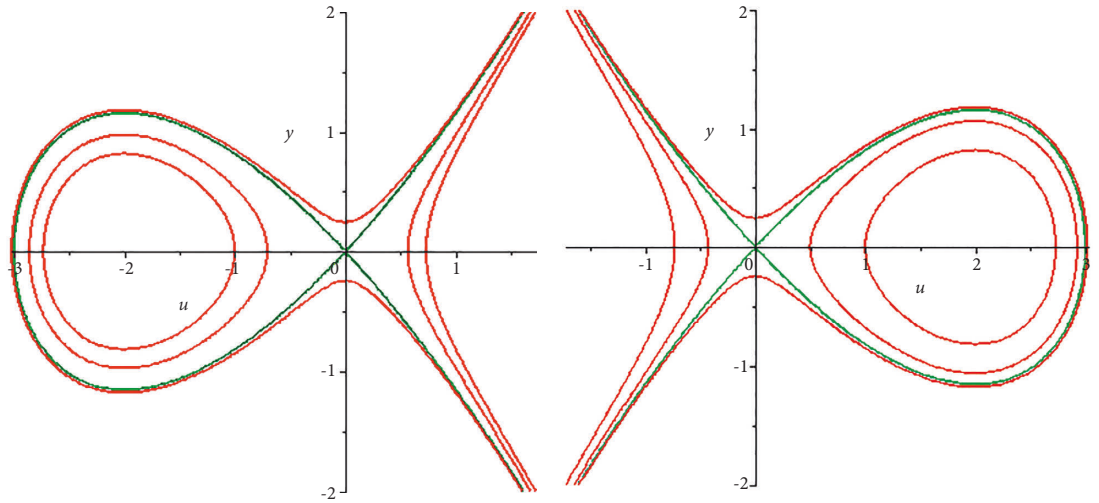

Figure 1: The phase portraits of the prototype equation (4) for $Q > 0$; (a) $R > 0$; (b) $R < 0$.

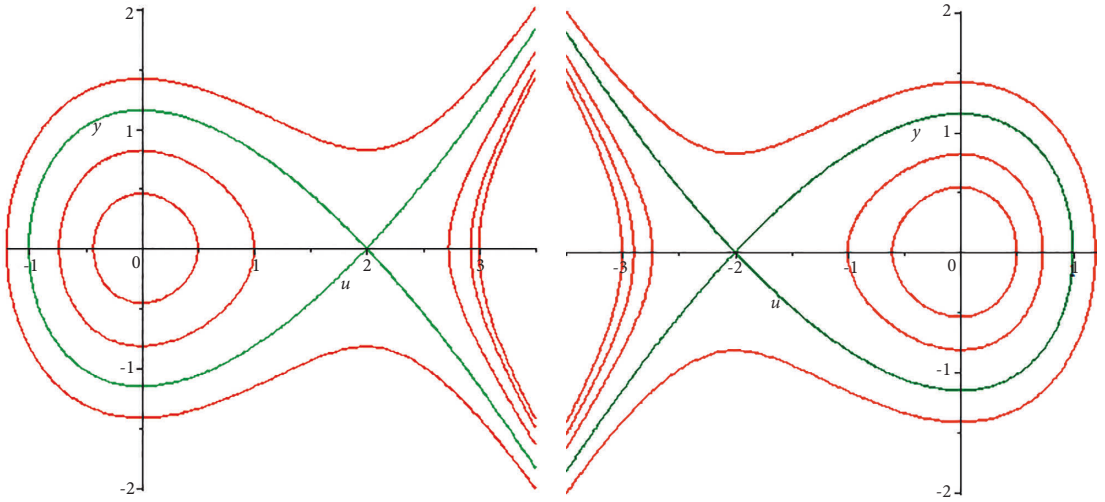

Figure 2: The phase portraits of the prototype equation (4) for $Q < 0$; (a) $R > 0$; (b) $R < 0$.

serve the condition $-Q/2R = \Theta_1 < U < \Theta_2 (= Q/R) < \Theta_3$.Combining the first equation of the prototype equations (4) and (11), we attain the parametric formulation of the periodic solution as follows:

$$U(x,t) = \Theta_1 + (\Theta_2 - \Theta_1) sn^2\left(\sqrt{\frac{R(\Theta_3 - \Theta_1)}{6}}\,|\xi|, \sqrt{\frac{(\Theta_2 - \Theta_1)}{(\Theta_3 - \Theta_1)}}\right). \tag{11}$$

The shape of the periodic outcomes of (12) is displayed in Figure 4(c) with $\omega = 1, \kappa = -1, Q = 1, R = 0.5$.

For the state $Q > 0$, $R < 0$, similar investigation can be used in Figure 1(b). Suppose, $(\Theta_4, 0)$, $(\Theta_5, 0)$ and $(\Theta_6, 0)$ are the meeting points of the curve identified by the orbits $H(U,V) = \hbar$, $\hbar \in (\hbar_1, 0)$ on the U -axis that preserve the condition $Q/2R = \Theta_4 < U < \Theta_5 < \Theta_6$.

We acquire the parametric formulation of the periodic solution as follows:

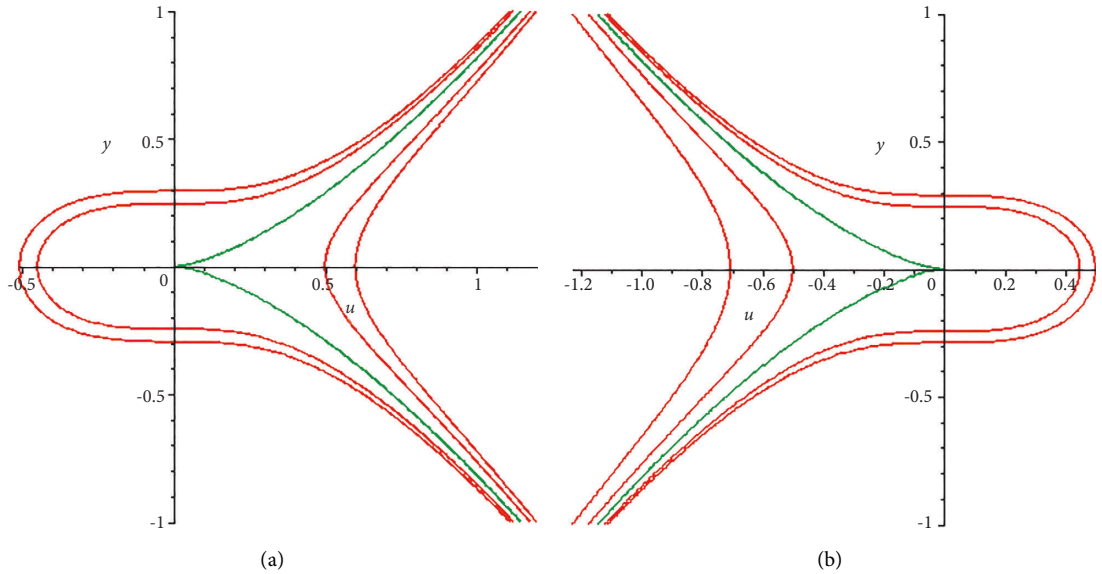

Figure 3: The phase portraits of the prototype equation (4) for $Q = 0$; (a) $R > 0$; (b) $R < 0$.

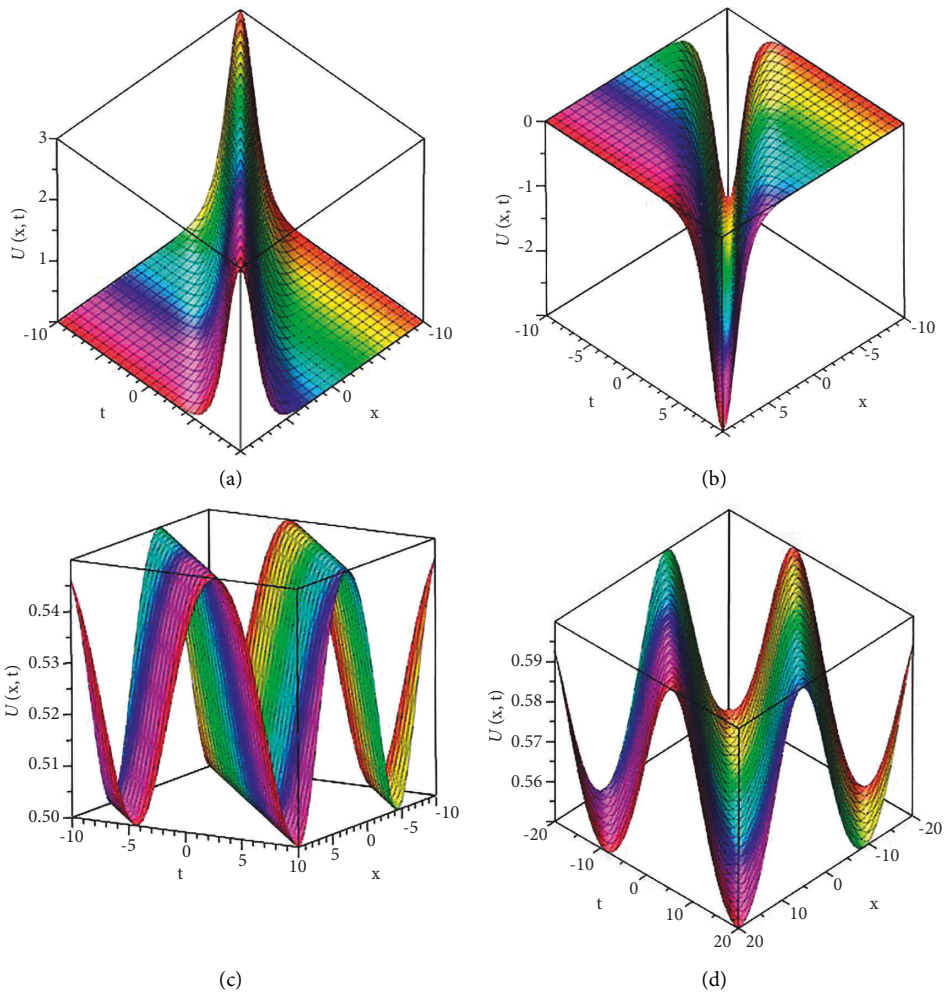

Figure 4: Shapes of the solutions. (a) Bright bell wave of equation (8), (b) dark bell wave of equation (10), (c) periodic wave of equation (12), and (d) periodic wave of equation (13).

$$U(x,t) = \Theta_4 + \frac{(\Theta_4 - \Theta_5)(\Theta_6 - \Theta_4)}{(\Theta_6 - \Theta_5)\, sn^2\left(\sqrt{R(\Theta_4 - \Theta_6)/6}\,|\xi|, \sqrt{(\Theta_6 - \Theta_5)/(\Theta_6 - \Theta_4)}\right) - (\Theta_6 - \Theta_4)}. \quad (12)$$

The shape of the periodic outcomes of (13) is presented in Figure 4(d) with $\omega = 1, \kappa = -1, Q = 1,\ R = 0.5$.

3.2. Examining Group-2 Based on Figure 2 Observation (Part 2)

(I) For the state $Q < 0,\ R > 0$, it is equivalent to the homoclinic orbit at the stable point $N_1(Q/R, 0)$ identified by $H(U,V) = \hbar_1$ where the prototype (4) suggests itself as a smooth solitary wave solution of valley type as depicted in Figure 2(a). With the help of the relation $H(U,V) = \hbar_1$ yields

$$V^2 = \frac{2R}{3}\left(U + \frac{Q}{R}\right)^2\left(U - \frac{Q}{2R}\right). \quad (13)$$

Then, by means of the first equation of the prototype (4) and (14), we attain the parametric expression of the valley-type smooth solitary wave solution that has a similar nature as depicted in Figure 4(a) as follows:

$$U(x,t) = \left|\frac{Q}{2R}\right|\left(1 - 3\tanh^2\left(\frac{\sqrt{-Q}}{2}|\xi|\right)\right), \quad (14)$$

where $\xi = \kappa x - \omega t,\quad P = \alpha/\omega\beta, Q = 1/\kappa^2\beta, R = 1/2\,\kappa\omega\beta$

(II) For the state $Q < 0,\ R < 0$, it is related to the homoclinic orbit at the stable point $N_1(Q/R, 0)$ identified by $H(U,V) = \hbar_1$, where the model (1) represents a valley-type smooth solitary wave solution as displayed in Figure 2(b). With the help of the relation $H(U,V) = \hbar_1$, yields

$$V^2 = -\frac{2R}{3}\left(U + \frac{Q}{R}\right)^2\left(\frac{Q}{2R} - U\right). \quad (15)$$

Then, by means of the first equation of the prototype (4) and (16), we attain the parametric expression of the valley-type smooth solitary wave solution that has similar nature as depicted in Figure 4(b) as follows:

$$U(x,t) = \left|\frac{Q}{2R}\right|\left(3\tanh^2\left(\frac{\sqrt{-Q}}{2}|\xi|\right) - 1\right), \quad (16)$$

where $\xi = \kappa x - \omega t,\quad P = \alpha/\omega\beta, Q = 1/\kappa^2\beta, R = 1/2\,\kappa\omega\beta$

(III) For the state $Q < 0,\ R > 0$ or $Q < 0,\ R < 0$, the prototype (4) has a group of smooth periodic wave solutions identified by $H(U,V) = \hbar,\ \hbar \in (0, \hbar_1)$, which can be observed in Figures 2(a) and 2(b), respectively. For this aspect, the formulation of the periodic solution is identical to the solutions in (12) and (13).

3.3. Examining Group-3 Based on Figure 3 Observation (Part 2).

(I) For the state $Q = 0,\ R > 0$, there is an unrestricted orbit with the alike Hamiltonian as the origin $N_0(0, 0)$ (Figure 3(a)). The open cusp orbit can be specified by

$$V^2 = \frac{2R}{3}U^3. \quad (17)$$

Then, by means of the first equation of the prototype (4) and (18), we acquire the periodic cusp wave solution as follows:

$$U(x,t) = \frac{6}{|R|\,\xi^2}, \quad (18)$$

where $\xi = \kappa x - \omega t,\quad P = \alpha/\omega\beta, Q = 1/\kappa^2\beta, R = 1/2\,\kappa\omega\beta$

The shape of the singular bright cusp wave of (19) is depicted in Figure 5(a) $a = -1,\ b = 1, \omega = 1, \kappa = 1,\ P = -1,\ Q = 0,\ R = 0.5$.

(II) For the state $Q = 0,\ R < 0$, there is also an unrestricted orbit with the alike Hamiltonian as the origin $N_0(0, 0)$ (Figure 3(b)). Due to this condition, we also catch out the similar periodic cusp wave solution in the form as follows:

$$U(x,t) = -\frac{6}{|R|\xi^2}, \quad (19)$$

where $\xi = \kappa x - \omega t,\ P = \alpha/\omega\beta, Q = 1/\kappa^2\beta, R = 1/2\kappa\omega\beta$

The profile of the singular dark cusp wave solution in (20) is depicted in Figure 5(b) $a = -1,\ b = 1, \omega = 1,\ \kappa = 1, P = -1,\ Q = 0,\ R = -0.5$.

4. Solutions of the Oskolkov Model via the Unified Method and Graphical Illustration

Let us apply a steadfast treatment of the unified method [32, 33] to the (1 + 1) dimensional Oskolkov model (1) in this portion. Graphical presentations are also outlined here.

4.1. Solutions of the Oskolkov Model. Using the travelling wave variable, we reinstate (1) into the ODE (2). Next, we enumerate the balance number of expressions in (2) between the linear term, U'' and the nonlinear term, U^2 by letting $N = 2$. Through this effort, a trial solution can be formed as follows:

$$U(\xi) = a_0 + a_1 S(\xi) + a_2 S(\xi)^2 + b_1 S(\xi)^{-1} + b_2 S(\xi)^{-2}. \quad (20)$$

Here $a_i, b_i; i = 0, 1, 2$ are unfamiliar constants to be formed subsequently and we consider the derivative of $S(\xi)$ satisfying an ODE namely the Riccati differential equation

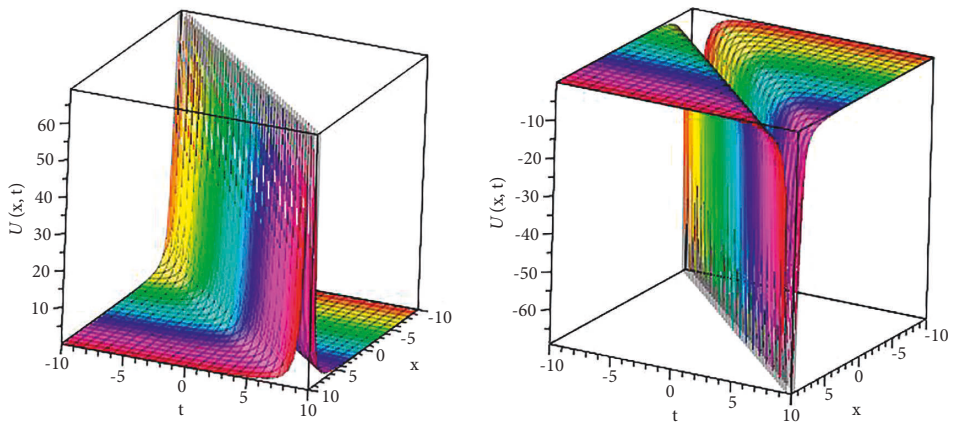

Figure 5: Shapes of the solutions. (a) Bright cusp wave of equation (19) and (b) dark cusp wave of equation (20).

$$S' = S(\xi)^2 + \lambda. \tag{21}$$

The solutions of the given Riccati equation are given as follows:

$$S(\xi) = \begin{cases} \dfrac{\sqrt{-\left(l^2 + d^2\right)\lambda} - l\sqrt{-\lambda}\cosh\left(2\sqrt{-\lambda}\,(\xi + E)\right)}{l\sinh\left(2\sqrt{-\lambda}\,(\xi + E)\right) + d}, \\ \dfrac{-\sqrt{-\left(l^2 + d^2\right)\lambda} - l\sqrt{-\lambda}\cosh\left(2\sqrt{-\lambda}\,(\xi + E)\right)}{l\sinh\left(2\sqrt{-\lambda}\,(\xi + E)\right) + d}, \\ \sqrt{-\lambda} + \dfrac{-2l\sqrt{-\lambda}}{l + \cosh\left(2\sqrt{-\lambda}\,(\xi + E)\right) - \sinh\left(2\sqrt{-\lambda}\,(\xi + E)\right)}, \\ -\sqrt{-\lambda} + \dfrac{2l\sqrt{-\lambda}}{l + \cosh\left(2\sqrt{-\lambda}\,(\xi + E)\right) + \sinh\left(2\sqrt{-\lambda}\,(\xi + E)\right)}. \end{cases} \tag{22}$$

Case-01: hyperbolic function (when $\lambda < 0$) as follows:

Case-02: trigonometric function (when $\lambda > 0$) as follows:

$$S(\xi) = \begin{cases} \dfrac{\sqrt{\left(l^2 - d^2\right)\lambda} - l\sqrt{\lambda}\cos\left(2\sqrt{\lambda}\,(\xi + E)\right)}{l\sin\left(2\sqrt{\lambda}\,(\xi + E)\right) + d}, \\ \dfrac{-\sqrt{\left(l^2 - d^2\right)\lambda} - l\sqrt{\lambda}\cos\left(2\sqrt{\lambda}\,(\xi + E)\right)}{l\sin\left(2\sqrt{\lambda}\,(\xi + E)\right) + d}, \\ i\sqrt{\lambda} + \dfrac{-2li\sqrt{\lambda}}{l + \cos\left(2\sqrt{\lambda}\,(\xi + E)\right) - i\sin\left(2\sqrt{\lambda}\,(\xi + E)\right)}, \\ -i\sqrt{\lambda} + \dfrac{2li\sqrt{\lambda}}{l + \cos\left(2\sqrt{\lambda}\,(\xi + E)\right) + i\sin\left(2\sqrt{\lambda}\,(\xi + E)\right)}, \end{cases} \tag{23}$$

where $l \neq 0$ and d, $S(\xi)$ are real arbitrary constants.

Case-03: rational function solutions (when $\lambda = 0$.)

$$S(\xi) = \frac{1}{\xi + E}. \tag{24}$$

Differentiating (21) as many times as necessary while satisfying (22), these expressions are substituted back into (1). Next, we attain a polynomial of $S(\xi)^J$ where $(J = \pm 0, \pm 1, \pm 2, \ldots, \pm N)$, and then by letting the coefficients of $S(\xi)^J$ equal to zero yields as follows:

$$\begin{aligned}
S^4(\xi)&: \frac{1}{2}ka_2^2 + 6\beta k^2\omega a_2 = 0,\\
S^3(\xi)&: ka_1a_2 - 2\alpha k^2a_2 + 2\beta k^2\omega a_1 = 0,\\
S^2(\xi)&: 8\beta k^2\omega a_2\lambda + ka_0a_2 - \alpha k^2a_1 + \frac{1}{2}ka_1^2 - \omega a_2 = 0,\\
S^1(\xi)&: ka_2b_1 + ka_0a_1 - 2\alpha k^2a_2\lambda + 2\beta k^2\omega a_1\lambda - \omega a_1 = 0,\\
S^0(\xi)&: 2\beta k^2\omega b_2 - \alpha k^2a_1\lambda + 2\beta k^2\omega a_2\lambda^2 + \alpha k^2b_1 + ka_2b_2 - \omega a_0 + ka_1b_1 + \frac{1}{2}ka_0^2 = 0,\\
S^{-1}(\xi)&: 2\alpha k^2b_2 + 2\beta k^2\omega b_1\lambda - \omega b_1 + +ka_1b_2 + ka_0b_1 = 0,\\
S^{-2}(\xi)&: -\omega b_2 + 8\beta k^2\omega b_2\lambda + ka_0b_2 + \frac{1}{2}kb_1^2 + \alpha k^2b_1\lambda = 0,\\
S^{-3}(\xi)&: 2\beta k^2\omega b_1\lambda^2 + 2\alpha k^2b_2\lambda + kb_1b_1 = 0,\\
S^{-4}(\xi)&: \frac{1}{2}kb_2^2 + 6\beta k^2\omega b_2\lambda^2 = 0.
\end{aligned} \tag{25}$$

By solving the above system of equations, many sets of solutions can be attained as follows:

Set-01:

$$\begin{aligned}
k &= \frac{1}{24}\sqrt{\frac{-6}{\beta\lambda}},\\
\omega &= \frac{\alpha}{20\beta}\sqrt{\frac{-1}{\lambda}},\\
a_0 &= \frac{\alpha}{4}\sqrt{\frac{6}{\beta}},\\
a_1 &= \frac{\alpha}{10}\sqrt{\frac{-6}{\beta\lambda}},\\
a_2 &= -\frac{\alpha}{40}\sqrt{\frac{-6}{\beta\lambda}}\sqrt{\frac{-1}{\lambda}},\\
b_1 &= \frac{-\alpha}{10}\sqrt{\frac{-6\lambda}{\beta}},\\
b_2 &= \frac{-3\lambda\alpha}{20}\sqrt{\frac{1}{\beta}}.
\end{aligned} \tag{26}$$

Set-02:

$$\begin{aligned}
k &= \frac{1}{24}\sqrt{\frac{6}{\beta\lambda}},\\
\omega &= \frac{\alpha}{20\beta}\sqrt{\frac{-1}{\lambda}},\\
a_0 &= \frac{3\alpha}{20}\sqrt{\frac{-6}{\beta}},\\
a_1 &= \frac{\alpha}{10}\sqrt{\frac{6}{\beta\lambda}},\\
a_2 &= -\frac{\alpha}{40}\sqrt{\frac{6}{\beta\lambda}}\sqrt{\frac{-1}{\lambda}},\\
b_1 &= \frac{-\alpha}{10}\sqrt{\frac{6\lambda}{\beta}},\\
b_2 &= \frac{-\lambda\alpha}{40}\sqrt{\frac{-6}{\beta}}.
\end{aligned} \tag{27}$$

Set-03:

$$k = \frac{1}{12}\sqrt{\frac{-6}{\beta\lambda}},$$
$$\omega = \frac{\alpha}{10\beta}\sqrt{\frac{-1}{\lambda}},$$
$$a_0 = \frac{3\alpha}{10}\sqrt{\frac{6}{\beta}},$$
$$a_1 = \frac{\alpha}{5}\sqrt{\frac{-6}{\beta\lambda}},$$
$$a_2 = -\frac{\alpha}{10}\sqrt{\frac{-6}{\beta\lambda}}\sqrt{\frac{-1}{\lambda}},$$
$$b_1 = b_2 = 0. \tag{28}$$

Set-04:

$$k = \frac{1}{12}\sqrt{\frac{6}{\beta\lambda}},$$
$$\omega = \frac{\alpha}{10\beta}\sqrt{\frac{-1}{\lambda}},$$
$$a_0 = \frac{\alpha}{10}\sqrt{\frac{-6}{\beta}},$$
$$a_1 = \frac{\alpha}{5}\sqrt{\frac{6}{\beta\lambda}},$$
$$a_2 = -\frac{\alpha}{10}\sqrt{\frac{6}{\beta\lambda}}\sqrt{\frac{-1}{\lambda}},$$
$$b_1 =$$
$$b_2 = 0. \tag{29}$$

Set-05:

$$k = \frac{1}{12}\sqrt{\frac{-6}{\beta\lambda}},$$
$$\omega = \frac{\alpha}{10\beta}\sqrt{\frac{-1}{\lambda}},$$
$$a_0 = \frac{3\alpha}{10}\sqrt{\frac{6}{\beta}},$$
$$b_1 = -\frac{\alpha}{5}\sqrt{\frac{-6\lambda}{\beta}},$$
$$b_2 = \frac{\lambda\alpha}{10}\sqrt{\frac{6}{\beta}},$$
$$a_1 = a_2 = 0. \tag{30}$$

Set-06:

$$k = \frac{1}{12}\sqrt{\frac{6}{\beta\lambda}},$$
$$\omega = \frac{\alpha}{10\beta}\sqrt{\frac{-1}{\lambda}},$$
$$a_0 = \frac{\alpha}{10}\sqrt{\frac{-6}{\beta}},$$
$$b_1 = -\frac{\alpha}{5}\sqrt{\frac{6\lambda}{\beta}},$$
$$b_2 = -\frac{\lambda\alpha}{10}\sqrt{\frac{-6}{\beta}},$$
$$a_1 = a_2 = 0. \tag{31}$$

Now, by plugging these expressions into (21) for unfamiliar constants, different types of solutions for (1) can be acquired.

For the Set-01, if $\lambda < 0$, then we obtain the hyperbolic function solutions

$$U_{1,1}(\xi) = \frac{\alpha}{4}\sqrt{\frac{6}{\beta}} + \frac{\alpha}{10}\sqrt{\frac{-6}{\beta\lambda}}\left(\frac{\sqrt{-\left(l^2+d^2\right)\lambda} - l\sqrt{-\lambda}\cosh\left(2\sqrt{-\lambda}\,(\xi+E)\right)}{l\sinh\left(2\sqrt{-\lambda}\,(\xi+E)\right)+d}\right)$$
$$-\frac{\alpha}{40}\sqrt{\frac{-6}{\beta\lambda}}\sqrt{\frac{-1}{\lambda}}\left(\frac{\sqrt{-(l^2+d^2)\lambda} - l\sqrt{-\lambda}\cosh\left(2\sqrt{-\lambda}\,(\xi+E)\right)}{l\sinh\left(2\sqrt{-\lambda}\,(\xi+E)\right)+d}\right)^2$$
$$-\frac{\alpha}{10}\sqrt{\frac{-6\lambda}{\beta}}\left(\frac{\sqrt{-(l^2+d^2)\lambda} - l\sqrt{-\lambda}\cosh\left(2\sqrt{-\lambda}\,(\xi+E)\right)}{l\sinh\left(2\sqrt{-\lambda}\,(\xi+E)\right)+d}\right)^{-1}$$
$$-\frac{3\lambda\alpha}{20}\sqrt{\frac{1}{\beta}}\left(\frac{\sqrt{-(l^2+d^2)\lambda} - l\sqrt{-\lambda}\cosh\left(2\sqrt{-\lambda}\,(\xi+E)\right)}{l\sinh\left(2\sqrt{-\lambda}\,(\xi+E)\right)+d}\right)^{-2}.$$

$$U_{1,2}(\xi) = \frac{\alpha}{4}\sqrt{\frac{6}{\beta}} + \frac{\alpha}{10}\sqrt{\frac{-6}{\beta\lambda}}\left(\frac{-\sqrt{-\left(l^2+d^2\right)\lambda} - l\sqrt{-\lambda}\cosh\left(2\sqrt{-\lambda}\,(\xi+E)\right)}{l\sinh\left(2\sqrt{-\lambda}\,(\xi+E)\right)+d}\right)$$
$$-\frac{\alpha}{40}\sqrt{\frac{-6}{\beta\lambda}}\sqrt{\frac{-1}{\lambda}}\left(\frac{-\sqrt{-(l^2+d^2)\lambda} - l\sqrt{-\lambda}\cosh\left(2\sqrt{-\lambda}\,(\xi+E)\right)}{l\sinh\left(2\sqrt{-\lambda}\,(\xi+E)\right)+d}\right)^2$$
$$-\frac{\alpha}{10}\sqrt{\frac{-6\lambda}{\beta}}\left(\frac{-\sqrt{-(l^2+d^2)\lambda} - l\sqrt{-\lambda}\cosh\left(2\sqrt{-\lambda}\,(\xi+E)\right)}{l\sinh\left(2\sqrt{-\lambda}\,(\xi+E)\right)+d}\right)^{-1}$$
$$-\frac{3\lambda\alpha}{20}\sqrt{\frac{1}{\beta}}\left(\frac{-\sqrt{-(l^2+d^2)\lambda} - l\sqrt{-\lambda}\cosh\left(2\sqrt{-\lambda}\,(\xi+E)\right)}{l\sinh\left(2\sqrt{-\lambda}\,(\xi+E)\right)+d}\right)^{-2}.$$

$$U_{1,3}(\xi) = \frac{\alpha}{4}\sqrt{\frac{6}{\beta}} + \frac{\alpha}{10}\sqrt{\frac{6}{\beta}}\left(1 + \frac{-2l}{l+\cosh\left(2\sqrt{-\lambda}\,(\xi+E)\right)-\sinh\left(2\sqrt{-\lambda}\,(\xi+E)\right)}\right)$$
$$-\frac{\alpha}{40}\sqrt{\frac{-6}{\beta\lambda}}\sqrt{\frac{-1}{\lambda}}\left(\sqrt{-\lambda} + \frac{-2l\sqrt{-\lambda}}{l+\cosh\left(2\sqrt{-\lambda\,(\xi+E)}\right)-\sinh\left(2\sqrt{-\lambda}\,(\xi\right.}\right.$$
$$-\frac{\alpha}{10}\sqrt{\frac{-6\lambda}{\beta}}\left(\sqrt{-\lambda} + \frac{-2l\sqrt{-\lambda}}{l+\cosh\left(2\sqrt{-\lambda}\,(\xi+E)\right)-\sinh\left(2\sqrt{-\lambda}\,(\xi+E\right.}\right.$$
$$-\frac{3\lambda\alpha}{20}\sqrt{\frac{1}{\beta}}\left(\sqrt{-\lambda} + \frac{-2l\sqrt{-\lambda}}{l+\cosh\left(2\sqrt{-\lambda}\,(\xi+E)\right)-\sinh\left(2\sqrt{-\lambda}\,(\xi+E\right.}\right.$$

$$U_{1,4}(\xi) = \frac{\alpha}{4}\sqrt{\frac{6}{\beta}} + \frac{\alpha}{10}\sqrt{\frac{6}{\beta}}\left(-1 + \frac{2l}{l+\cosh\left(2\sqrt{-\lambda}\,(\xi+E)\right)+\sinh\left(2\sqrt{-\lambda}\,(\xi+E)\right.}\right.$$
$$-\frac{\alpha}{40}\sqrt{\frac{-6}{\beta\lambda}}\sqrt{\frac{-1}{\lambda}}\left(-\sqrt{-\lambda} + \frac{2l\sqrt{-\lambda}}{l+\cosh\left(2\sqrt{-\lambda}\,(\xi+E)\right)+\sinh\left(2\sqrt{-\lambda}\,(\right.}\right.$$
$$-\frac{\alpha}{10}\sqrt{\frac{-6\lambda}{\beta}}\left(-\sqrt{-\lambda} + \frac{2l\sqrt{-\lambda}}{l+\cosh\left(2\sqrt{-\lambda}\,(\xi+E)\right)+\sinh\left(2\sqrt{-\lambda}\,(\xi+\right.}\right.$$
$$-\frac{3\lambda\alpha}{20}\sqrt{\frac{1}{\beta}}\left(-\sqrt{-\lambda} + \frac{2l\sqrt{-\lambda}}{l+\cosh\left(2\sqrt{-\lambda}\,(\xi+E)\right)+\sinh\left(2\sqrt{-\lambda}\,(\xi+E\right.}\right.$$

(32)

where $\xi = 1/24\sqrt{-6/\beta\lambda}\, x - \alpha/20\beta\sqrt{-1/\lambda}\, t$ while $l, d,\ E$ are arbitrary constants.

For the Set-01, if $\lambda > 0$, then we obtain trigonometric function solutions

$$
\begin{aligned}
U_{1,5}(\xi) &= \frac{\alpha}{4}\sqrt{\frac{6}{\beta}} + \frac{\alpha}{10}\sqrt{\frac{-6}{\beta\lambda}}\left(\frac{\sqrt{\left(l^2-d^2\right)\lambda}\ - l\sqrt{\lambda}\,\cos\left(2\sqrt{\lambda}\,(\xi+E)\right)}{l\,\sin\left(2\sqrt{\lambda}\,(\xi+E)\right)+d}\right)\\
&\quad - \frac{\alpha}{40}\sqrt{\frac{-6}{\beta\lambda}}\sqrt{\frac{-1}{\lambda}}\left(\frac{\sqrt{(l^2-d^2)\lambda}\ - l\sqrt{\lambda}\,\cos\left(2\sqrt{\lambda}\,(\xi+E)\right)}{l\,\sin\left(2\sqrt{\lambda}\,(\xi+E)\right)+d}\right)^2\\
&\quad - \frac{\alpha}{10}\sqrt{\frac{-6\lambda}{\beta}}\left(\frac{\sqrt{(l^2-d^2)\lambda}\ - l\sqrt{\lambda}\,\cos\left(2\sqrt{\lambda}\,(\xi+E)\right)}{l\,\sin\left(2\sqrt{\lambda}\,(\xi+E)\right)+d}\right)^{-1}\\
&\quad - \frac{3\lambda\alpha}{20}\sqrt{\frac{1}{\beta}}\left(\frac{\sqrt{(l^2-d^2)\lambda}\ - l\sqrt{\lambda}\,\cos\left(2\sqrt{\lambda}\,(\xi+E)\right)}{l\,\sin\left(2\sqrt{\lambda}\,(\xi+E)\right)+d}\right)^{-2}.\\
U_{1,6}(\xi) &= \frac{\alpha}{4}\sqrt{\frac{6}{\beta}} + \frac{\alpha}{10}\sqrt{\frac{-6}{\beta\lambda}}\left(\frac{-\sqrt{\left(l^2-d^2\right)\lambda}\ - l\sqrt{\lambda}\,\cos\left(2\sqrt{\lambda}\,(\xi+E)\right)}{l\,\sin\left(2\sqrt{\lambda}\,(\xi+E)\right)+d}\right)\\
&\quad - \frac{\alpha}{40}\sqrt{\frac{-6}{\beta\lambda}}\sqrt{\frac{-1}{\lambda}}\left(\frac{-\sqrt{(l^2-d^2)\lambda}\ - l\sqrt{\lambda}\,\cos\left(2\sqrt{\lambda}\,(\xi+E)\right)}{l\,\sin\left(2\sqrt{\lambda}\,(\xi+E)\right)+d}\right)^2\\
&\quad - \frac{\alpha}{10}\sqrt{\frac{-6\lambda}{\beta}}\left(\frac{-\sqrt{(l^2-d^2)\lambda}\ - l\sqrt{\lambda}\,\cos\left(2\sqrt{\lambda}\,(\xi+E)\right)}{l\,\sin\left(2\sqrt{\lambda}\,(\xi+E)\right)+d}\right)^{-1}\\
&\quad - \frac{3\lambda\alpha}{20}\sqrt{\frac{1}{\beta}}\left(\frac{-\sqrt{(l^2-d^2)\lambda}\ - l\sqrt{\lambda}\,\cos\left(2\sqrt{\lambda}\,(\xi+E)\right)}{l\,\sin\left(2\sqrt{\lambda}\,(\xi+E)\right)+d}\right)^{-2}.\\
U_{1,7}(\xi) &= \frac{\alpha}{4}\sqrt{\frac{6}{\beta}} + \frac{\alpha}{10}\sqrt{\frac{6}{\beta}}\left(1+\frac{-2l}{l+\cos\left(2\sqrt{\lambda}\,(\xi+E)\right)-i\,\sin\left(2\sqrt{\lambda}\,(\xi+E)\right)}\right)\\
&\quad - \frac{\alpha}{40}\sqrt{\frac{-6}{\beta\lambda}}\sqrt{\frac{-1}{\lambda}}\left(i\sqrt{\lambda}+\frac{-2li\sqrt{\lambda}}{l+\cos\left(2\sqrt{\lambda}\,(\xi+E)\right)-i\,\sin\left(2\sqrt{\lambda}\,(\xi+E)\right)}\right)^2\\
&\quad - \frac{\alpha}{10}\sqrt{\frac{-6\lambda}{\beta}}\left(i\sqrt{\lambda}+\frac{-2li\sqrt{\lambda}}{l+\cos\left(2\sqrt{\lambda}\,(\xi+E)\right)-i\,\sin\left(2\sqrt{\lambda}\,(\xi+E)\right)}\right)^{-1}\\
&\quad - \frac{3\lambda\alpha}{20}\sqrt{\frac{1}{\beta}}\left(i\sqrt{\lambda}+\frac{-2li\sqrt{\lambda}}{l+\cos\left(2\sqrt{\lambda}\,(\xi+E)\right)-i\,\sin\left(2\sqrt{\lambda}\,(\xi+E)\right)}\right)^{-2}.\\
U_{1,8}(\xi) &= \frac{\alpha}{4}\sqrt{\frac{6}{\beta}} + \frac{\alpha}{10}\sqrt{\frac{-6}{\beta\lambda}}\left(-i\sqrt{\lambda}+\frac{2li\sqrt{\lambda}}{l+\cos\left(2\sqrt{\lambda}\,(\xi+E)\right)+i\,\sin\left(2\sqrt{\lambda}\,(\xi+E)\right)}\right)\\
&\quad - \frac{\alpha}{40}\sqrt{\frac{-6}{\beta\lambda}}\sqrt{\frac{-1}{\lambda}}\left(-i\sqrt{\lambda}+\frac{2li\sqrt{\lambda}}{l+\cos\left(2\sqrt{\lambda}\,(\xi+E)\right)+i\,\sin\left(2\sqrt{\lambda}\,(\xi+E)\right)}\right)^2\\
&\quad - \frac{\alpha}{10}\sqrt{\frac{-6\lambda}{\beta}}\left(-i\sqrt{\lambda}+\frac{2li\sqrt{\lambda}}{l+\cos\left(2\sqrt{\lambda}\,(\xi+E)\right)+i\,\sin\left(2\sqrt{\lambda}\,(\xi+E)\right)}\right)^{-1}\\
&\quad - \frac{3\lambda\alpha}{20}\sqrt{\frac{1}{\beta}}\left(-i\sqrt{\lambda}+\frac{2li\sqrt{\lambda}}{l+\cos\left(2\sqrt{\lambda}\,(\xi+E)\right)+i\,\sin\left(2\sqrt{\lambda}\,(\xi+E)\right)}\right)^{-2},
\end{aligned}
\tag{33}
$$

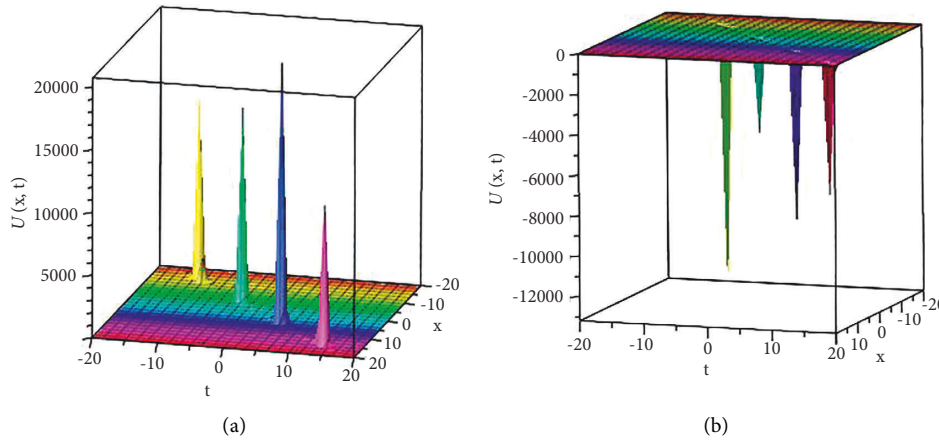

(a) (b)

FIGURE 6: (a) $U_{1,1}$, (b) $U_{1,2}$ with parameters $\lambda = -0.5, \alpha = 1, \beta = 0.2, d = 1, E = 0.5, l = 2$.

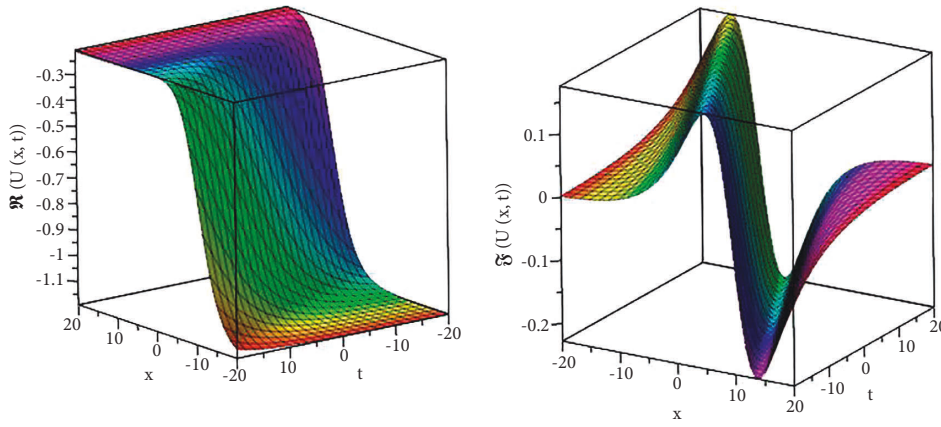

(a) (b)

FIGURE 7: (a) Real and (b) imaginary parts of $U_{1,5}$ for $\lambda = 2, \alpha = -1, \beta = 1, d = 1, E = 3, l = 2$.

where $\xi = 1/24\sqrt{-6/\beta\lambda}\, x - \alpha/20\beta\sqrt{-1/\lambda}\, t$ while $l \neq 0$, d and E are real arbitrary constants.

If $\lambda = 0$, we can search out rational function type solutions, but in this case, if we consider $\lambda = 0$ then the executed values of k, ω, a_2, b_1 and b_2 will be undefined. So, the solution is rejected. Similarly, the other sets (Set-02 to Set-06) each provide us with eight solutions in the same way.

4.2. Numerical Illustrations of the Obtained Results and Discussion. In this section, we will deliberate the nature and behavior of all the solutions physically with 2-D and 3-D graphs, as well as density plots of the $(1 + 1)$ dimensional Oskolkov model by instigating the most recent method, namely, the unified method. The solution $U_{1,1}$ conveys the multipeaked bright solitonic nature for the parametric values $\lambda = -0.5, \alpha = 1, \beta = 0.2, d = 1, E = 0.5, l = 2$. Oppositely, the solution $U_{1,2}$ conveys the multipeaked dark solitonic nature for the parametric values $\lambda = -0.5, \alpha = 1, \beta = 0.2, d = 1, E = 0.5, l = 2$ as illustrated in Figure 6. The real part of $U_{1,5}$ presents the kink type shock wave whereas its imaginary part presents the combo bright-dark bell wave for the parameters $\lambda = 2, \alpha = -1, \beta = 1, d = 1, E = 3, l = 2$ as illustrated in Figure 7. On the other hand, the real part of $U_{1,6}$ conveys the combo dark-bright bell wave with a shock wave, whereas its imaginary part expresses the bright bell wave with a shock for the parameter $\lambda = 2, \alpha = \beta = 1, d = 3, E = -3, l = 2$, as illustrated in Figure 8. The real part of the solution $U_{1,7}$ presents the dark bell as a double shock wave but its imaginary part presents the double bright-dark bell wave with a shock for the parameters $\lambda = 2, \alpha = \beta = 1, d = 3, E = -3, l = 2$, as demonstrated in Figure 9. The real part of $U_{1,8}$ conveys the bright bell wave with double shocks but its imaginary part conveys the bright-dark bell wave with a shock for the parametric values $\lambda = 2, \alpha = -1, \beta = 1, d = 3, E = -3, l = 2$, as demonstrated in Figure 10. Both the real and imaginary parts of $U_{5,5}$ represents the multi-rogue type waves with singularities for $\lambda = 2, \alpha = 1, \beta = 0.2, d = 1, E = -1, l = -2$, as demonstrated in Figure 11. Yet, every solution obtained for the model by using this technique can be reduced to the multirogue (bright-dark) type wave with the changing signs of the

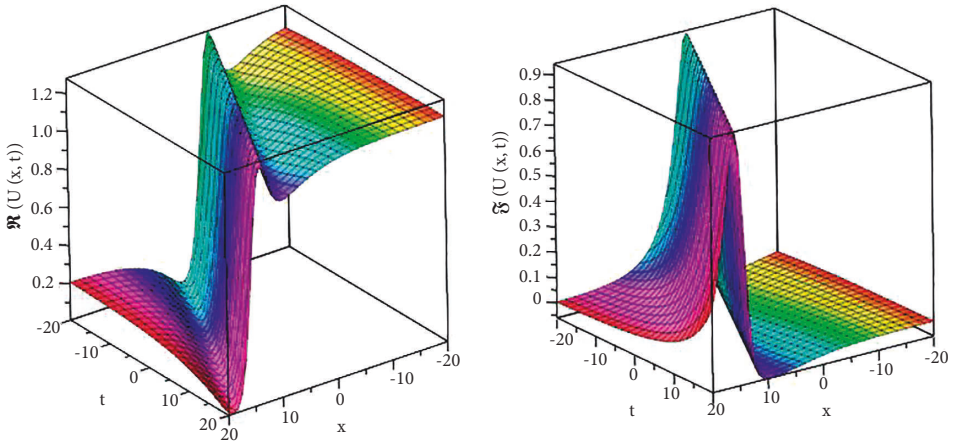

(a) (b)

Figure 8: (a) Real and (b) imaginary parts of $U_{1,6}$ for $\lambda = 2, \alpha = \beta = 1, d = 3, E = -3, l = 2$.

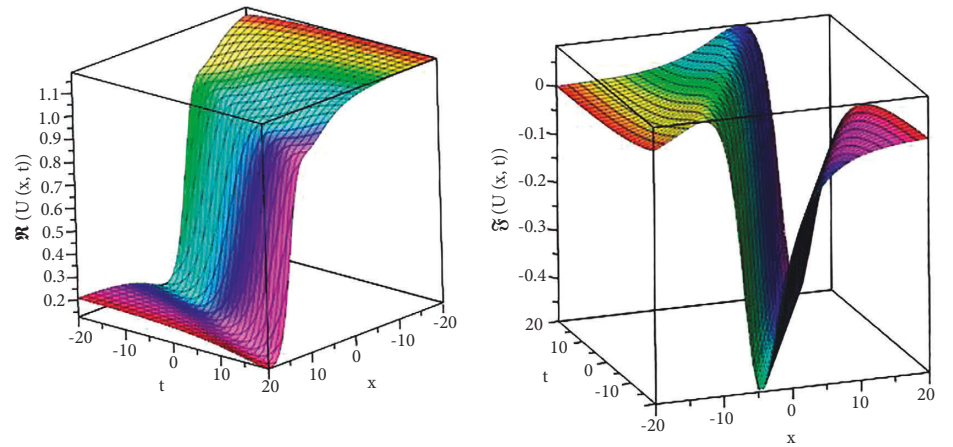

(a) (b)

Figure 9: (a) Real and (b) imaginary parts of $U_{1,7}$ for $\lambda = 2, \alpha = \beta = 1, d = 3, E = -3, l = 2$.

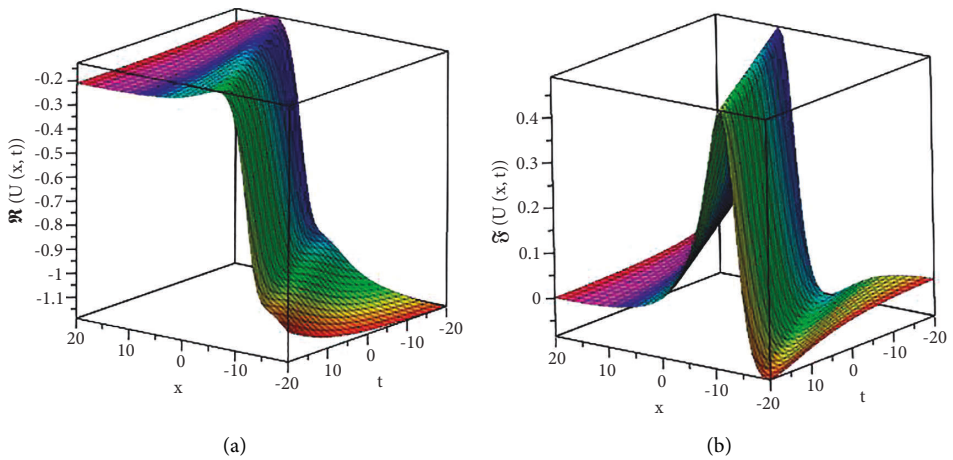

(a) (b)

Figure 10: (a) Real and (b) imaginary parts of $U_{1,8}$ for $\lambda = 2, \alpha = -1, \beta = 1, d = 3, E = -3, l = 2$.

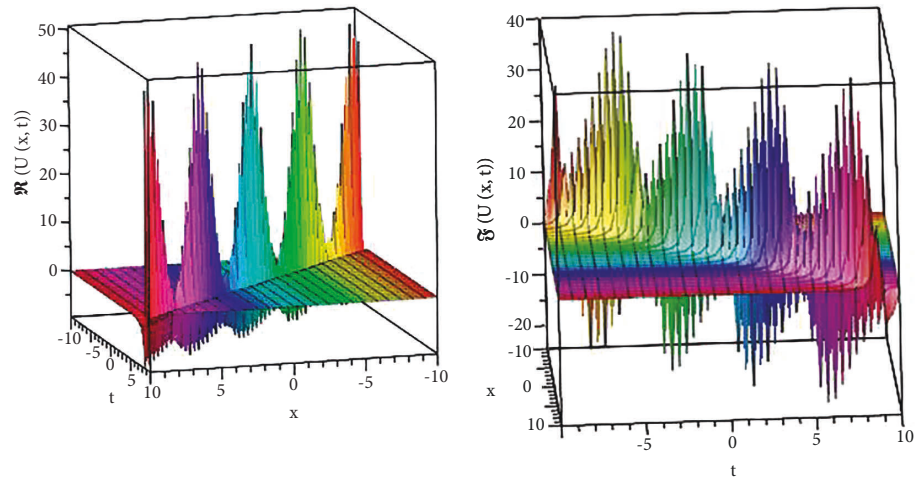

(a) (b)

FIGURE 11: (a) Real and (b) imaginary parts of $U_{5,5}$ for $\lambda = 2, \alpha = 1, \beta = 0.2, d = 1, E = -1, l = -2$.

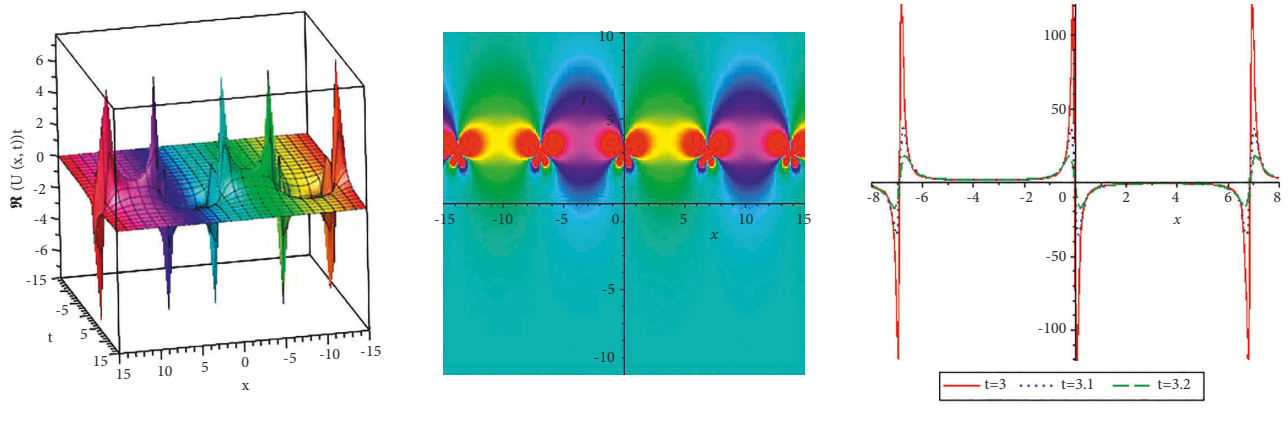

(a) (b) (c)

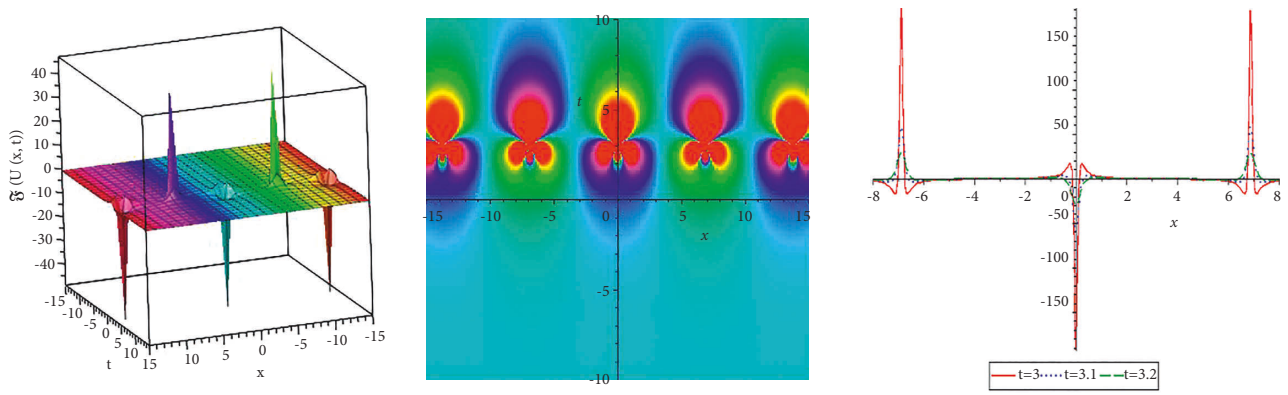

(a) (b) (c)

FIGURE 12: (a) Real and (b) imaginary parts (upper plots for real and lower plots for the imaginary part) of $U_{2,1}$ for $\lambda = -1, \alpha = -1, \beta = 0.2, d = 1, E = 0, l = 0.5$ and (c) 2D plot of the graph at $t = 0$.

parameters β and E. Such a dynamic is displayed in Figure 12 of the solution $U_{2,1}$ for the parametric values $\lambda = -1, \alpha = -1, \beta = 0.2, d = 1, E = 0, l = 0.5$. Besides, we display its density and 2D plots of corresponding real and imaginary parts altogether.

5. Conclusions

Through this work, the key effort is to procure, test, and explore the innovative travelling wave solutions and the physical properties of the nonlinear Oskolkov model for

Kevin-Voigt fluids by utilizing two reliable mathematical techniques. Based on the bifurcation theory of the dynamical scheme, we explored the bifurcation and derived a phase portrait of the model using diverse parametric conditions. We have derived smooth bright bell and dark bell waves, periodic solutions as well as singular dark cusp and bright cusp waves. These travelling waves are achieved by corresponding to homoclinic, periodic, and open orbits with the cusp of each orbit of the phase portraits, respectively. The unified method as a substantial way to derive the new travelling wave solutions has been utilized through which we have successfully achieved the solutions for multipeaked bright and dark solitons, shock waves, bright bell waves with a shock, bright bell waves with a double shock, combo bright-dark and dark-bright bell waves with a shock, dark bell into a double shock wave, and bright-dark multirogue type waves. The bifurcation analysis of this model is presented first in this article, even though most of the obtained solutions derived by direct integration from the Hamiltonian of the model according to each energy is the first step here. In particular, the bright bell waves with a shock, bright bell waves with double shock, combo bright-dark, combo dark-bright bell waves with a shock, dark bell into a double shock wave, and bright-dark multirogue type waves were not reported in the previous literature. This technique proposes solutions with free parameters that could be significant to deliberate more intricate nonlinear corporal phenomena. The obtained solutions in this paper reaffirmed that the method is very effective and easily applicable to formulate more exact travelling wave solutions than other methods of the nonlinear evolution models occurring in many mathematical physics and engineering applications.

Data Availability

The data used to support the findings of this study are included in the article.

Conflicts of Interest

The authors declare that they have no conflicts of interest.

References

[1] E. Yasar, Y. Yıldırım, and A. R. Adem, "Perturbed optical solitons with spatio-temporal dispersion in (2 + 1)-dimensions by extended Kudryashov method," *Optik*, vol. 158, pp. 1–14, 2018.

[2] G. Akram and N. Mahak, "Application of the first integral method for solving (1 + 1) dimensional cubic-quintic complex Ginzburg–Landau equation," *Optik*, vol. 164, pp. 210–217, 2018.

[3] Z. J. Xiao, B. Tian, H. L. Zhen, J. Chai, and X. Y. Wu, "Multi-soliton solutions and Bäcklund transformation for a two-mode KdV equation in a fluid," *Waves in Random and Complex Media*, vol. 27, no. 1, pp. 1–14, 2016.

[4] X. W. Yan, S. F. Tian, M. J. Dong, and L. Zou, "Bäcklund transformation, rogue wave solutions and interaction phenomena for a $$\varvec{(3+1)}$$ (3 + 1) -dimensional B-type Kadomtsev–Petviashvili–Boussinesq equation," *Nonlinear Dynamics*, vol. 92, no. 2, pp. 709–720, 2018.

[5] B. Nawaz, K. Ali, S. T. R. Rizvi, and M. Younis, "Soliton solutions for quintic complex Ginzburg-Landau model," *Superlattices and Microstructures*, vol. 110, pp. 49–56, 2017.

[6] S. Bilige and C. Temuer, *Applied Mathematics and Computation*, vol. 216, pp. 3146–3153, 2016.

[7] H. O. Roshid, "Novel solitary wave solution in shallow water and ion acoustic plasma waves in-terms of two nonlinear models via MSE method," *Journal of Ocean Engineering and Science*, vol. 2, no. 3, pp. 196–202, 2017.

[8] H. O. Roshid, M. M. Roshid, N. Rahman, and M. R. Pervin, "New solitary wave in shallow water, plasma and ion acoustic plasma via the GZK-BBM equation and the RLW equation," *Propulsion and Power Research*, vol. 6, no. 1, pp. 49–57, 2017.

[9] H. O. Roshid and W. X. Ma, *Physics Letters*, vol. 382, no. 45, pp. 3262–3268, 2018.

[10] M. B. Hossen, H. O. Roshid, and M. Z. Ali, "Characteristics of the solitary waves and rogue waves with interaction phenomena in a (2 + 1)-dimensional Breaking Soliton equation," *Physics Letters A*, vol. 382, no. 19, pp. 1268–1274, 2018.

[11] H. Naher and F. A. Abdullah, "New generalized (G'/G)-expansion method to the zhiber-shabat equation and liouville equations," *Journal of Physics: Conference Series*, vol. 890, p. 012018, 2017.

[12] M. M. Roshid and H. O. Roshid, "Exact and explicit traveling wave solutions to two nonlinear evolution equations which describe incompressible viscoelastic Kelvin-Voigt fluid," *Heliyon*, vol. 4, no. 8, p. e00756, 2018.

[13] S. Akter, R. K. Sen, and H. O. Roshid, "Dynamics of interaction between solitary and rogue wave of the space-time fractional Broer–Kaup models arising in shallow water of harbor and coastal zone," *SN Applied Sciences*, vol. 2, no. 12, p. 2000, 2020.

[14] R. Reza and S. Abazari, *Mathematical and Computer Modelling*, vol. 52, pp. 1834–1845, 2010.

[15] A. A. N. Stéphane, D. Augustin, and M. B. César, "Extended (G'/G) method applied to the modified non-linear schrodinger equation in the case of ocean rogue waves," *Open Journal of Marine Science*, vol. 04, no. 04, pp. 246–256, 2014.

[16] A. M. Wazwaz, "Multiple soliton solutions for a (2+1)-dimensional integrable KdV6 equation," *Communications in Nonlinear Science and Numerical Simulation*, vol. 15, no. 6, pp. 1466–1472, 2010.

[17] M. Ikram, A. Muhammad, and A. Rahmn, "Analytic Solution To Benjamin-Bona-Mahony Equation By Using Laplace Adomian Decomposition Method," *Matrix Sci. Math.*vol. 3, no. 1, pp. 01–04, 2019.

[18] M. A. E. Abdelrahman, E. H. M. Zahran, and M. M. A. Khater, "The expansion method and its application for solving nonlinear evolution equations," *International Journal of Modern Nonlinear Theory and Application*, vol. 04, no. 01, pp. 37–47, 2015.

[19] A. Boz and A. Bekir, "Application of Exp-function method for (3+1) -dimensional nonlinear evolution equations," *Computers & Mathematics with Applications*, vol. 56, no. 5, pp. 1451–1456, 2008.

[20] M. M. A. Khater, "Exact traveling wave solutions for the generalized Hirota-Satsuma couple KdV system using the $\exp(-\varphi(\xi))$-expansion method," *Cogent Mathematics*, vol. 3, no. 1, p. 1172397, 2016.

[21] H. Bin, L. Jibin, L. Yao, and R. Weiguo, "Bifurcations of travelling wave solutions for a variant of Camassa–Holm equation," *Nonlinear Analysis: Real World Applications*, vol. 9, no. 2, pp. 222–232, 2008.

[22] Y. Zhou and Q. Liu, "World Real Analysis," *Abstract and Applied Analysis*, vol. 2012, p. 109235, 2012.
[23] O. F. Gözükızıl and S. Akçagıl, *Adva. Diff. Eqns.*vol. 143, p. 2013, 2013.
[24] G. A. Sviridyuk and A. S. Shipilov, "On the stability of solutions of the Oskolkov equations on a graph," *Differential Equations*, vol. 46, no. 5, pp. 742–747, 2010.
[25] A. Turgut, T. Aydemir, A. Saha, and A. H. Kara, "Propagation of nonlinear shock waves for the generalised Oskolkov equation and its dynamic motions in the presence of an external periodic perturbation," *Pramana - Journal of Physics*, vol. 90, pp. 78–90, 2018.
[26] L. L. Feng and T. T. Zhang, "Breather wave, rogue wave and solitary wave solutions of a coupled nonlinear Schrödinger equation," *Applied Mathematics Letters*, vol. 78, pp. 133–140, 2018.
[27] S. Xu and J. He, "The rogue wave and breather solution of the Gerdjikov-Ivanov equation," *Journal of Mathematical Physics*, vol. 53, no. 6, p. 063507, 2012.
[28] Y. Yue, L. Huang, and Y. Chen, "N-solitons, breathers, lumps and rogue wave solutions to a (3+1)-dimensional nonlinear evolution equation," *Computers & Mathematics with Applications*, vol. 75, no. 7, pp. 2538–2548, 2018.
[29] M. Onorato, S. Residori, U. Bortolozzo, A. Montina, and F. T. Arecchi, "Rogue waves and their generating mechanisms in different physical contexts," *Physics Reports*, vol. 528, no. 2, pp. 47–89, 2013.
[30] Z. Rahman, M. Z. Ali, H. O. Roshid, M. S. Ullah, and X. Y. Wen, "Dynamical structures of interaction wave solutions for the two extended higher-order KdV equations," *Pramana - Journal of Physics*, vol. 95, no. 3, p. 134, 2021.
[31] H. O. Roshid, M. S. Khatun, N. F. M. Noor, H. M. Baskonus, and F. B. M. Belgacem, "Commun. Nonl. Sci. Numer," *Simuletter*, vol. 101, p. 105867, 2021.
[32] P. Sunthrayuth, N. H. Aljahdaly, A. Ali, R. Shah, I. Mahariq, and A. M. J. Tchalla, *Journal of Function Spaces*, vol. 2021, pp. 2021–14, 2021.
[33] F. M. Alharbi, A. M. Zidan, M. Naeem, R. Shah, and K. Nonlaopon, *Journal of Function Spaces*, vol. 2021, pp. 2021–14, 2021.
[34] N. H. Aljahdaly, A. Akgu¨l, R. Shah, I. Mahariq, and J. Kafe, "Investigation of rest," *Journal of Mathematics*, vol. 8876149, p. 2022, 2022.
[35] M. Areshi, A. Khan, R. Shah, and K. Nonlaopon, "Analytical investigation of fractional-order Newell-Whitehead-Segel equations via a novel transform," *AIMS Mathematics*, vol. 7, no. 4, pp. 6936–6958, 2022.
[36] M. K. Alaoui, R. Fayyaz, A. Khan, R. Shah, and M. S. Abdo, "Analytical investigation of noyes–field model for time-fractional belousov–zhabotinsky reaction," *Complexity*, vol. 2021, pp. 3248376–21, 2021.
[37] P. Sunthrayuth, R. Ullah, A. Khan et al., "Numerical analysis of the fractional-order nonlinear system of volterra integro-differential equations," *Journal of Function Spaces*, vol. 2021, pp. 2021–10, 2021.
[38] S. Akcagil and T. Aydemir, "A new application of the unified method," *NTMSCI*, vol. 1, no. 6, pp. 185–199, 2018.
[39] O. F. Gozukızıl, S. Akcagıl, and T. Aydemir, "Unification of all hyperbolic tangent function methods," *Open Physics*, vol. 14, no. 1, pp. 524–541, 2016.